

# RSDet++: Point-based Modulated Loss for More Accurate Rotated Object Detection

Wen Qian, Xue Yang, Silong Peng, Junchi Yan *Member, IEEE*, Xiujuan Zhang

**Abstract**—We classify the discontinuity of loss in both five-param and eight-param rotated object detection methods as rotation sensitivity error (RSE) which will result in performance degeneration. We introduce a novel modulated rotation loss to alleviate the problem and propose a rotation sensitivity detection network (RSDet) which consists of an eight-param single-stage rotated object detector and the modulated rotation loss. Our proposed RSDet has several advantages: 1) it reformulates the rotated object detection problem as predicting the corners of objects while most previous methods employ a five-param regression method with different measurement units. 2) modulated rotation loss achieves consistent improvement on both five-param and eight-param rotated object detection methods by solving the discontinuity of loss. To further improve the accuracy of our method on objects smaller than 10 pixels, we introduce a novel RSDet++ which consists of a point-based anchor-free rotated object detector and a modulated rotation loss. Extensive experiments demonstrate the effectiveness of both RSDet and RSDet++, which achieve competitive results on rotated object detection in the challenging benchmarks DOTA1.0, DOTA1.5, and DOTA2.0. We hope the proposed method can provide a new perspective for designing algorithms to solve rotated object detection and pay more attention to tiny objects. The codes and models are available at: <https://github.com/yangxue0827/RotationDetection>.

**Index Terms**—Rotated object detection; Modulated loss; Point-based; Tiny objects

## I. INTRODUCTION

Object detection is one of the fundamental tasks in computer vision, which motivates many downstream vision applications such as re-identification, semantic segmentation, and face recognition. Usual object detectors employ horizontal bounding boxes to describe the position of predicted objects, where the candidates of the center point, width, and height are sufficient to locate them efficiently. However, it is challenging for them to detect those rotated, dense, and tiny objects accurately. For example, recently many rotated object detection benchmarks such as aerial dataset (DOTA [1], UCAS-AOD [2], HRSC2016 [3]), scene text dataset (ICDAR2015 [4], ICDAR2017 [5]) have been published. Intuitively, the rotated object detection that provides more accurate position descriptions can solve the above problem. We aim to design a more reasonable loss function for an effective rotated object detector, which provides a rotated object detection baseline.

Wen Qian, Silong peng (Corresponding author) are with Institute of Automation, Chinese Academy of Sciences, and also with the University of Chinese Academy of Sciences. Xue Yang, Junchi Yan are with Department of Computer Science and Engineering, Shanghai Jiao Tong University. Xiujuan Zhang is with the Inner Mongolia Key Laboratory of Molecular Biology on Featured Plants.

E-mail: {qianwen2018, silong.peng}@ia.ac.cn, {yangxue-2019-sjtu, yanjunchi}@sjtu.edu.cn, mingyuesong@163.com

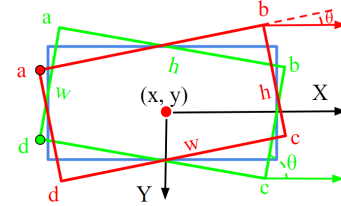


Fig. 1. Loss discontinuity: rectangles in blue, red, and green denote reference box, ground truth, and prediction respectively. Here the reference box is rotated one degree clockwise to get the ground truth and is rotated similarly counterclockwise to obtain the prediction. Then the three boxes are described with five parameters: reference  $(0, 0, 10, 25, -90^\circ)$ , ground truth  $(0, 0, 25, 10, -1^\circ)$ , and prediction  $(0, 0, 10, 25, -89^\circ)$ . Here  $\ell_1$  loss is far more than 0.

The definition of parameters for rotated object detection has a significant effect on final prediction results, and most of the rotated object detectors can be classified as five-parameter or eight-parameter methods based on their parameterization approaches. Five-parameter methods use coordinates of the central point, width, height, and rotation angle to describe the position and orientation of the rotated bounding box. However, traditional five-parameter rotated object detection methods have several drawbacks which will influence the final performance, and we classify them as: 1) the discontinuity of loss 2) the inconsistency units of regression parameters. The discontinuity of loss mainly results by the contradiction between the parameterization of the rotated bounding box and the loss function, which both neglect the boundary situation during the regression process and lead to a value mutation of loss during training (see Fig. 1). Moreover, the parameters, i.e., angle, width, height, and candidates of central point have different measurement units and lead to several relations against the Intersection over Union (IoU). These parameters result in inconsistent loss values while previous works add them directly without any specification, which leads to a performance decrease.

Although eight-parameter methods use the coordinates of corners as the regression parameters based on consistent units, a similar discontinuity of loss still exists in eight-parameter ones. The corner order changes with slightly angular disturbance near the boundary position, and the computation of loss can not hold this situation adaptively.

As mentioned before, the discontinuity of loss exists in both five-parameter methods and eight-parameter methods and we summarize this phenomenon as rotation sensitivity error (RSE). RSE can result in loss mutation when going through the boundary position, and can lead to training instability (see Fig. 10). In order to address the rotation sensitivity error, we propose a novel modulated rotation loss  $\ell_{mr}$  which handles

the boundary constraints for rotation carefully, leading to a smoother loss curve during the training process. In other words, we add a correction term to the original loss and take the minimum value between the primary one and the correction term. This correction is particularly greater than  $\ell_1$ -loss when it does not reach the range boundary of the angle. However, this correction becomes normal when  $\ell_1$ -loss undergoes a mutation. All in all, such correction can be seen as the symmetry of  $\ell_1$ -loss about the location of the mutation. Finally, the curve of  $\ell_{mr}$  is continuous after taking the minimum of  $\ell_1$ -loss and the correction term.

We instantiate our method based on the popular object detector RetinaNet weighting for the performance and speed, termed RSDet. It's easy to use other detectors (YOLO, Faster RCNN, SSD, CenterNet, and FCOS) as the backbone with just a few modifications. Recently, the rotated object detection benchmarks focus more on the tiny samples smaller than 10 pixels, and existing rotated object detectors are all anchor-based methods that have limited performance on these scenes. Anchor-based methods employ an FPN-architecture for multi-scale objects and use the lower layers to generate anchors for saving the computation cost. However, the ignorance of top feature maps will lead to performance damage since anchor-based methods map the samples by computing the Intersection over Union (IOU) between predicted and ground-truth boxes. The tiny ground truth will have a small IOU value with a large anchor, and no suitable anchor matched for the ground truth can be found. A similar phenomenon can also be found in our RSDet that some tiny objects will be ignored.

For further improving the performance on tiny samples, a point-based rotated object detection method based on modulated rotation loss is proposed, termed RSDet++. RSDet++ uses eight parameters to describe the bounding boxes of objects, which are regressed from a center-point instead of the anchor. We conduct the sample mapping process among ground truth and predictions in RSDet++ based on the distance among center point and ground-truth box, which gets rid of the errors from the IoU-based mapping process and improves the detection performance of tiny samples.

The preliminary content of this paper has partially appeared in AAAI 2021 [6]<sup>1</sup>. The overall contribution of this extended journal version can be summarized as:

i) We introduce the discontinuity of loss which exists in both five-parameter and eight-parameter rotated object detection methods, and formally formulate this phenomenon as rotation sensitivity error (RSE).

ii) For alleviating the RSE in the widely used five-parameter and eight-parameter systems, we devise a special treatment to ensure the loss continuity. We term the new loss as modulated rotation loss  $\ell_{mr}$ .

<sup>1</sup>To obtain a more thorough analysis and comprehensive results on tiny objects, the conference version has been significantly extended and improved in the journal version, especially in the following aspects: i) we point out that anchor-based rotated object detection methods show poor performance on tiny objects, and propose a novel anchor-free RSDet++ to solve the problem; ii) we use modulated rotation loss in RSDet++, which reaches consistent improvement in anchor-based method; iii) we use more challenging datasets to verify the performance on tiny objects, such as DOTA1.5 and DOTA2.0, which contain more tiny objects.

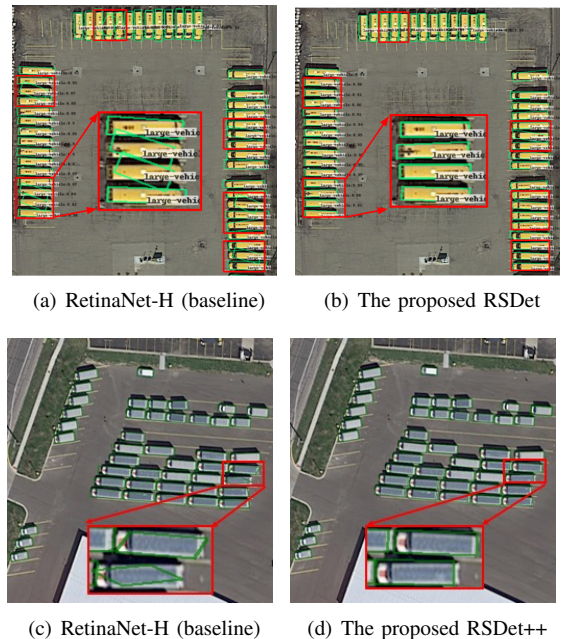


Fig. 2. Detection results before and after solving the RSE problem with RSDet and RSDet++. The red rectangles in (a) and (c) represent failed examples due to the discontinuity of loss.

iii) To further improve the performance of the rotated object detection methods on tiny samples, we propose RSDet++ based on the point-based bounding box regression method and modulated rotation loss.

## II. RELATED WORK

We emphasize two problems of rotated object detection in this paper: the discontinuity of loss and the ignorance of tiny objects. We analyze whether these problems existing in horizontal object detection methods and why they occur in rotated object detections. Finally, some methods that focus on a similar problem with us are introduced.

a) *Horizontal Object Detectors*: Visual object detection has been a hot topic over the decades. Since the seminal work R-CNN [7], there have been a series of improvements including Fast RCNN [8], Faster RCNN [9], and R-FCN [10], which fall into the category of the two-stage methods. On the other hand, people develop single-stage approaches which are more efficient than the two-stage methods. Examples include Overfeat [11], YOLO [12], and SSD [13]. In particular, SSD [13] combines the advantages of Faster RCNN and YOLO to achieve the trade-off between speed and accuracy. Subsequently, multi-scale feature fusion techniques are widely adopted in both single-stage methods and two-stage ones, such as FPN [14], RetinaNet [15], and DSSD [16]. Recently, researchers put forward many cascaded or refined detectors. For example, Cascade RCNN [17], HTC [18], and FSCascade [19] perform multiple classifications and regressions in the second stage, leading to notable accuracy improvements in both localization and classification. Besides, the anchor free methods have become a new research focus, including FCOS [20], FoveaBox [21], and RepPoints [22]. People simplify the structures of these detectors by discarding anchors,

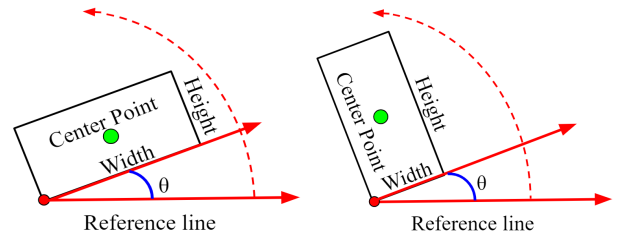
so anchor-free methods have opened up a new direction for object detection.

However, the above detectors only generate horizontal bounding boxes, which limit their applicability in many real-world scenarios. The objects in scene texts or aerial images tend to be densely arranged and have large aspect ratios, which requires more accurate localization. Therefore, rotated object detection has become a prominent direction in recent studies [22]. Moreover, the aforementioned horizontal object detection methods [7], [12], [13], [15] use four parameters (coordinates of the center point, width, and height) to describe the position of an object, which represent different physical meanings with no boundary condition needs to be considered. For improving the performance on small objects, horizontal object detection methods usually use the FPN as backbone [10], [14], and a cascaded network architecture [17], [18], [19] is usual.

*b) Rotated Object Detectors:* Rotated object detection usually uses an extra angle parameter to describe the orientation of an object or use the coordinates of four vertices which embedding the orientation information, and rotated bounding boxes can provide a more accurate position description than horizontal bounding boxes. Rotated object detection has been widely used in natural scene text [23], [24], aerial imagery [25], [26], [27], etc. People introduce many excellent detectors for scene text. For example, RRPN [24] uses rotating anchors to improve the qualities of region proposals. R<sup>2</sup>CNN [23] is a multi-tasking text detector that simultaneously detects rotated and horizontal bounding boxes. In TextBoxes++ [28], a long convolution kernel is used to accommodate the slenderness of the text with the number of proposals increasing.

Moreover, object detection in aerial images is more challenging for the complex backgrounds, dense arrangements, and a high proportion of small objects. Many scholars have also applied general object detection algorithms to aerial images, and many robust rotated detectors have emerged. For example, ICN [29] combines various modules such as image pyramid, feature pyramid network, and deformable inception sub-networks, and it achieves satisfactory performances on the DOTA benchmark. RoI Transformer [30] extracts rotation-invariant features for boosting subsequent classification and regression. SCRDet [31] proposes an IoU-smooth  $\ell_1$  loss to solve the sudden loss change caused by the angular periodicity so that it can better handle small, cluttered, and rotated objects. R<sup>3</sup>Det [32] proposes an end-to-end refined single-stage rotated object detector for fast and accurate object localization by solving the feature misalignment problem.

*c) The ignored boundary condition:* All the above mentioned rotated object detectors [23], [30], [32] do not take the inherent discontinuity of loss into account, which can damage learning stability and final detection performances in our experiments. However, no existing studies have addressed this fundamental problem that motivates our work. Moreover, we notice some works deal with a similar problem with us. SCRDet [31] combines the IOU-loss and smooth L1 loss, and the IoU-smooth L1 loss partly circumvents the need for differentiable rotating IoU loss. Gliding vertex [33] and CenterMap [34] use quadrilateral and mask to accurately



(a) Width is longer than height. (b) Height is longer than width.

Fig. 3. The five-parameter definition in OpenCV exchanges the width and the height in the boundary condition for rotation. The angle parameter  $\theta$  ranges from  $-90$  degree to  $0$  degree, but it should be distinguished from another definition [1], with  $180$  degree angular range, whose  $\theta$  is determined by long side of rectangle and x-axis.

describe oriented objects, respectively. CLS [35] transforms angular prediction from a regression problem to a classification one. We operate a comparison between our RSDet and the above methods, which shows that our method outperforms them.

### III. METHODOLOGY

Firstly, we reformulate popular rotated object detection methods can be classified as five-parameter methods and eight-parameter methods, and summarize the discontinuity of loss as the rotation sensitivity error which commonly exists in previous methods in section 3.1. Secondly, we introduce a modulated rotation loss to alleviate the rotation sensitivity loss and propose the RSDet based on modulated rotation loss in section 3.2. Finally, we propose RSDet++, which employs a point-based bounding box regression method to improve the detection performance on tiny objects.

#### A. Parameterization of Rotated Bounding Box

*1) Five-parameter Methods:* Given a rotated object, and we aim to describe its position and orientation by five parameters: the coordinates  $(x, y)$  of the center point, the width  $w$ , and the height  $h$  for the positional description; the rotation angle  $\theta$  for the orientation description. This kind of definition is in line with that in OpenCV as shown in Fig. 3, while the width  $w$  and the height  $h$  are related to the angle  $\theta$ : a) define the reference line along the horizontal direction that locates the vertex with the smallest vertical coordinate. b) rotate the reference line counterclockwise, the first rectangular side that be got to by the reference line is width  $w$  regardless of its length compared with the other side – height  $h$ . c) the central point coordinate is  $(x, y)$ , and the rotation angle is  $\theta$ .

Although some previous rotated object detection methods such as R<sup>2</sup>CNN [23], RRPN [24], ICN [29], and FFA [36] all employ the five parameter parameterization and achieve great improvements when comparing with traditional methods. There also exist some shortcomings which have negative impacts on detection performance:

The inconsistent of parameter units: different measurement units of five parameters lead to inconsistent regression processes, and the impact of such artifacts has rarely been studied in the literature. We analyze the relationships among all the parameters and IoU empirically in Fig. 4. Specifically, the

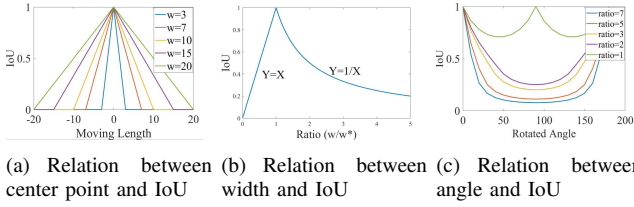


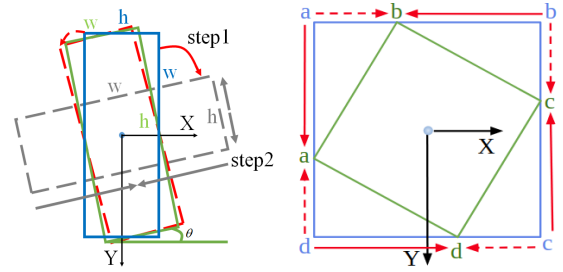
Fig. 4. Inconsistency in five-parameter regression model. The relationship between height and IoU is similar to relationship between width and IoU.

relationship between IoU and width (height) behaves like a combination of a linear function and an inverse proportion function, as illustrated in Fig. 4(a). The relationship between the central point and IoU is a symmetric linear function, as illustrated in Fig. 4(b). Completely different from other parameters, the relationship between the angle parameter and IoU is a multiple polynomial function (see Fig. 4(c)). Such regression inconsistency is highly likely to deteriorate the training convergence and the detection performance. Note that we use IoU as the standard measurement since that the final detection performance depends on whether IoU between the prediction and ground truth is high enough.

The discontinuity of loss: the angle parameter is the main reason for the loss discontinuity. To obtain the predicted box that coincides with the ground truth box, the horizontal reference box rotates counterclockwise, as shown in Fig. 5. In this figure, the coordinates of the predicted box are transformed from those of the blue reference box  $(0, 0, 100, 25, -90^\circ)$  to  $(0, 0, 100, 25, -100^\circ)$  in the normal coordinate system. However, the angle of the predicted box is out of the defined range, and the actual coordinates of the green ground truth box are  $(0, 0, 25, 100, -10^\circ)$ . Although the rotation process is physically smooth, the loss becomes large since the discontinuity of loss. To avoid such a loss fluctuation, the reference box need to be rotated clockwise to obtain the gray box  $(0, 0, 100, 25, -10^\circ)$  in Fig. 5(a) (step 1), then width and height of the gray box will be scaled to obtain the red predicted box  $(0, 0, 25, 100, -10^\circ)$  (step 2). At this time, although the loss value is close to zero, the detector experiences a complex regression. The above process requires relatively high robustness, which increases the training difficulty. More importantly, More importantly, an explicit and specific way for achieving a smooth regression process is needed.

2) *Eight-parameter Methods.*: Instead of the above five-parameter methods, the eight-parameter method employs the coordinates of vertexes to describe the position and orientation of rotated objects. To be consistent with the description, we order the four vertexes as following: a) starting from the lower-left corner a) b) four clockwise vertexes (a, b, c, d) of the rotated bounding box are used to describe its location, as shown in Fig. 1. In fact, such a parameterization protocol is convenient for quadrilateral description, which is friendly in more complex application scenarios.

Although the parameter units of eight-parameter methods are consistent, we find that the loss discontinuity also exists. Supposing that a ground truth box can be described with the corner sequence  $a \rightarrow b \rightarrow c \rightarrow d$  (see red box in Fig. 1). However, the corner sequence becomes  $d \rightarrow a \rightarrow b \rightarrow c$  (see



(a) 5-parameter regression w/ two steps in boundary condition procedure (b) Eight-parameter regression

Fig. 5. Boundary discontinuity analysis of five-parameter regression and eight-parameter regression. The red solid arrow indicates the actual regression process, and the red dotted arrow indicates the ideal regression process.

green box in Fig. 1) when the ground truth box undergoes a slightly angle change. Therefore, consider the situation of an eight-parameter regression in the boundary case, as shown in Fig. 5(b). The actual regression process from the blue reference box to the green ground truth box is  $\{(a \rightarrow a), (b \rightarrow b), (c \rightarrow c), (d \rightarrow d)\}$ , but apparently the ideal regression process should be  $\{(a \rightarrow b), (b \rightarrow c), (c \rightarrow d), (d \rightarrow a)\}$ . This situation also causes the regression process more difficult and unstable.

3) *Rotation Sensitivity Error.*: Based on the above analysis of five-parameter and eight-parameter methods, we conclude the discontinuity of loss as the rotation sensitivity error in rotated object detection. The existing rotated bounding box definition method is modified from previous horizontal object detection, and it is unsuitable for rotated object detection.

The coordinates of the object center  $(x, y)$ , the width  $w$ , and the height  $h$  for horizontal object position description are independent and have exclusive physical meaning. However, the definition of the width  $w$  and the height  $h$  are dependent on the angle  $\theta$  in five-parameter methods, while the coordinates of vertexes in the eight-parameter mode share the same physical meaning and confuse the loss computation process. When computing for the rotated object detection losses, the parameters for the predicted bounding box and the ground-truth box may be misaligned near the boundary condition for the ASE, which leads to the discontinuity of loss.

## B. Our Proposed Modulated loss

Two kinds of approaches are employed to solve the rotation sensitivity error (RSE): 1) a novel definition for the rotated bounding box which can avoid the rotation sensitivity error; 2) correcting the boundary condition through loss function based on existing parameterization methods. Considering that there are many existing rotated detection methods based on five-parameter or eight-parameter parameterization, we propose modulated rotation loss  $\ell_{mr}$  to solve RSE in this section. The pseudo equation of  $\ell_{mr}$  can be described as:

$$\ell_{mr} = \min \left\{ \begin{array}{l} \ell_1(P_r, T) \\ \ell_1(P_m, T) \end{array} \right. \quad (1)$$

where  $P_r$  and  $P_m$  represent the original predicted box and the modulated predicted box,  $T$  represents the ground-truth or label, and  $\ell_1$  represents for the least absolute error.

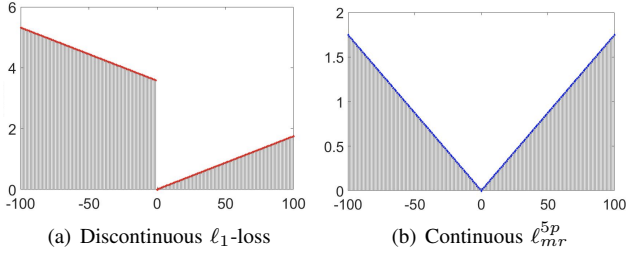


Fig. 6. Comparison of loss continuity between two kinds of loss functions.

1) *Five-parameter Modulated Rotation Loss*: As mentioned above, RSE only occurs in the boundary cases (see Fig. 6(a)). In this paper, we devise the following boundary constraints to modulate the loss as termed by modulated rotation loss  $\ell_{mr}^{5p}$ :

$$\ell_{cp} = |x_1 - x_2| + |y_1 - y_2|, \quad (2)$$

$$\ell_{mr}^{5p} = \min \begin{cases} \ell_{cp} + |w_1 - w_2| + |h_1 - h_2| + |\theta_1 - \theta_2| \\ \ell_{cp} + |w_1 - h_2| + |h_1 - w_2| \\ \quad + |90 - |\theta_1 - \theta_2||, \end{cases} \quad (3)$$

where  $\ell_{cp}$  is the central point loss. The first item in  $\ell_{mr}$  is  $\ell_1$ -loss. The second item is a correction used to make the loss continuous by eliminating the angular periodicity and the exchangeability of height and width. This correction is particularly larger than  $\ell_1$ -loss when it does not reach the range boundary of the angle parameter. However, this correction becomes normal when  $\ell_1$ -loss changes abruptly. In other words, such correction can be seen as the symmetry of  $\ell_1$ -loss about the location of the mutation. Finally,  $\ell_{mr}$  takes the minimum of  $\ell_1$ -loss and the correction term. The curve of  $\ell_{mr}$  is continuous, as sketched in Fig. 6(b).

In practice, the employment of relative values of bounding box regression can avoid the errors caused by objects on different scales. Therefore, the  $\ell_{mr}$  in this paper is:

$$\nabla \ell_{cp} = |t_{x1} - t_{x2}| + |t_{y1} - t_{y2}|, \quad (4)$$

$$\ell_{mr}^{5p} = \min \begin{cases} \nabla \ell_{cp} + |t_{w1} - t_{w2}| + |t_{h1} - t_{h2}| + |t_{\theta1} - t_{\theta2}| \\ \nabla \ell_{cp} + |t_{w1} - t_{h2} - \log(r)| \\ \quad + |t_{h1} - t_{w2} + \log(r)| + ||t_{\theta1} - t_{\theta2}| - \frac{\pi}{2}|, \end{cases} \quad (5)$$

where  $t_x = (x - x_a)/w_a$ ,  $t_y = (y - y_a)/h_a$ ,  $t_w = \log(w/w_a)$ ,  $t_h = \log(h/h_a)$ ,  $r = \frac{h}{w}$ ,  $t_\theta = \frac{\theta\pi}{180}$ . Here the measurement unit of the angle parameter is radian,  $r$  represents the aspect ratio.  $x$  and  $x_a$  are respectively the predicted box and the anchor box (likewise for  $y$ ,  $w$ ,  $h$ ,  $\theta$ ).

2) *Eight-parameter Modulated Rotation Loss*: The eight-parameter regression method means the prediction is a quadrilateral. Quadrilateral regression needs to sort the four corner points in advance, or else we will reach a huge loss value even if the position prediction is correct. For solving the ambiguity of point order, we propose an algorithm to get the sequence of four points (detailed implementation as shown in algorithm 1). Note that this algorithm is only for convex quadrilaterals and takes clockwise output as an example. The loss discontinuity phenomenon also exists in the eight-parameter regression

**Algorithm 1** Determination of the sequence of quadrilateral corner points.

---

**Input:** Four vertex vectors of quadrilateral  $\vec{p}_1, \vec{p}_2, \vec{p}_3, \vec{p}_4$   
**Output:** Four vertex vectors arranged clockwise  
 $\vec{p}'_1, \vec{p}'_2, \vec{p}'_3, \vec{p}'_4$

- 1:  $S \leftarrow \{\vec{p}_1, \vec{p}_2, \vec{p}_3, \vec{p}_4\}$ ,  $\vec{p}'_2 = \vec{p}'_3 = \vec{p}'_4 = \vec{0}$ ;
- 2:  $\vec{p}'_1 \leftarrow \text{FindLeftmostVertex}(S)$ ;
- 3:  $S \leftarrow S - \{\vec{p}'_1\}$
- 4: **for**  $\vec{s}_1 \in S$  **do**
- 5:      $\vec{s}_2, \vec{s}_3 \in S - \{\vec{s}_1\}$
- 6:     **if**  $\text{CrossProduct}(\vec{s}_1 - \vec{p}'_1, \vec{s}_2 - \vec{p}'_1) \times \text{CrossProduct}(\vec{s}_1 - \vec{p}'_1, \vec{s}_3 - \vec{p}'_1) < 0$  **then**
- 7:          $\vec{p}'_3 = \vec{s}_1$ ,  $S \leftarrow \{\vec{s}_2, \vec{s}_3\}$ ;
- 8:         **break**;
- 9:     **end if**
- 10: **end for**
- 11: **for**  $\vec{s}_1 \in S$  **do**
- 12:      $\vec{s}_1 = S - \{\vec{s}_1\}$ ;
- 13:     **if**  $\text{CrossProduct}(\vec{p}'_3 - \vec{p}'_1, \vec{s}_1 - \vec{p}'_1) > 0$  **then**
- 14:          $\vec{p}'_2 = \vec{s}_1$ ,  $\vec{p}'_4 = \vec{s}_2$ ;
- 15:     **else**
- 16:          $\vec{p}'_2 = \vec{s}_2$ ,  $\vec{p}'_4 = \vec{s}_1$ ;
- 17:     **end if**
- 18: **end for**
- 19: **return**  $\vec{p}'_1, \vec{p}'_2, \vec{p}'_3, \vec{p}'_4$

---

method, and we devise the eight-parameter version of our modulated rotation loss which consists of three components: i) move the four vertices of the predicted box clockwise by one place; ii) keep the order of the vertices of the predicted box unchanged; iii) move the four vertices of the predicted box counterclockwise by one place; iv) take the minimum value in the above three cases. Therefore,  $\ell_{mr}^{8p}$  can be expressed as:

$$\ell_{mr}^{8p} = \min \begin{cases} \sum_{i=0}^3 \left( \frac{|x_{(i+3)\%4} - x_i^*|}{w_a} + \frac{|y_{(i+3)\%4} - y_i^*|}{h_a} \right) \\ \sum_{i=0}^3 \left( \frac{|x_i - x_i^*|}{w_a} + \frac{|y_i - y_i^*|}{h_a} \right) \\ \sum_{i=0}^3 \left( \frac{|x_{(i+1)\%4} - x_i^*|}{w_a} + \frac{|y_{(i+1)\%4} - y_i^*|}{h_a} \right) \end{cases} \quad (6)$$

where  $x_i$  and  $y_i$  denote the  $i$ -th vertex coordinates of the predicted box and the reference box.  $x_i^*$ ,  $y_i^*$  respectively denote the  $i$ -th vertex coordinates of the ground truth box and the reference box.

Through the eight-parameter regression and the definition of  $\ell_{mr}^{8p}$ , the problems of the regression inconsistency and the loss discontinuity in rotation detection are eliminated. Extensive experiments show that our method is more stable for training (see Fig. 10) and outperforms other methods (as shown in Table VIII).

3) *RSDet based on Modulated Rotation loss*: The proposed RSDet is an effective and unified framework which consists of a backbone network, a definition specified head, and the

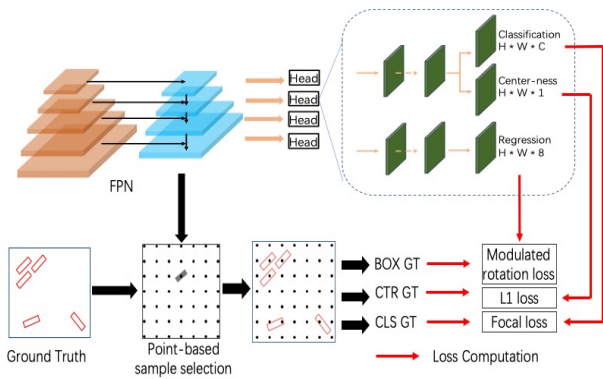


Fig. 7. The overview of RSDet++ framework. RSDet++ employs a point-based regression method to avoid the ignorance of tiny sample.

modulated rotation loss. To enable efficiency and performance, our backbone follows RetinaNet which is a representative method for one-stage object detection. We noticed that although the eight-parameter method has been proposed for a long time, few rotated detection methods use this for parameterization. RSDet provides two kinds of heads, a five-parameter regression one and an eight-parameter regression one, and we employ the modulated rotation loss to improve them.

### C. Modulated Loss in Anchor-free Method

It's challenging to apply our method on benchmarks such as DOTA1.5 and DOTA2.0 since many small objects smaller than 10 pixels are difficult to be detected, and we termed this phenomenon as tiny trouble. The tiny trouble also exists in anchor-based methods that tend to employ a pyramid architecture for performance improvement. Moreover, they usually set up anchors from the P3 stage because the large resolution of the P1 and P2 ones will result in unaffordable computational costs. We subsample the original image 8 times to get the P3 stage feature, and the objects smaller than 10 pixels will disappear after the subsampling operation. The anchor-based methods choose the positive/negative samples by calculating the IOU between the anchor set and the ground truth set, and too small objects will lead to a lower IOU value which is smaller than the threshold value. Some previous methods such as RoI transformer [30] propose to use a two-stage detection backbone and a larger feature map such as P2 to improve the small object detection performance, which is computational costing and time costing.

Inspired by the tiny trouble and the anchor-free based method, we propose an RSDet++ that regresses eight-parameter of four vertexes from a point and employs the modulated rotation loss for solving ASE. Instead of predefined anchors, RSDet++ regresses the eight-parameter values from each pixel on the feature maps and termed them as center points. RSDet++ chooses the positive and negative samples by the relationship between center points and ground truth boxes as show in 8(c). As the center points won't disappear with the subsampling of the feature map, so RSDet++ can alleviate the tiny trouble better. Specifically, the differences between the positive/negative chosen methods in anchor-based

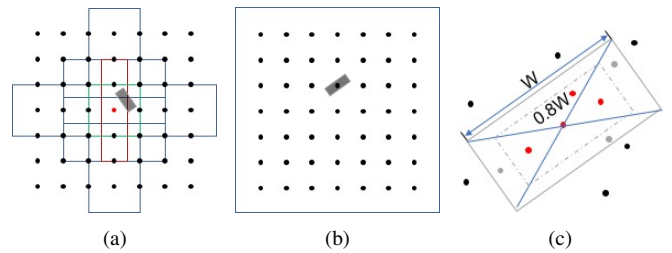


Fig. 8. Comparison of the positive/negative sample selection process between anchor-based and point-based methods. a) the positive/negative sample selection process in anchor-based methods by IoU computation. b/c) the positive/negative sample selection process in point-based methods.

and anchor-free methods are shown in Fig. 8. Finally, our RSDet++ shortens the training time and provides a faster inference time.

RSDet++ employs a point-based regression method to generate the proposals, which regresses all four vertexes coordinates from the same point. So each point on the feature map can be viewed as an anchor point, and we need to judge whether the point belongs to a target object or not. However, the IOU-based operation is employed to differentiate the positive sample and negative anchor in anchor-based methods, but it can't be applied to RSDet++ since no anchor exists. So a point-based positive and negative sample selection approach is selected, given an anchor point  $(x_a, y_a)$  and a target object  $(x_1, y_1; x_2, y_2; x_3, y_3; x_4, y_4)$ . If the point is outside the object region, it will be termed a negative point; and if it is inside the object region, it will be termed a positive point or an ignored one corresponding to the distance from the central point.

$$\begin{aligned} x_c &= (x_1 + x_2 + x_3 + x_4)/4; \\ y_c &= (y_1 + y_2 + y_3 + y_4)/4; \\ w &= \sqrt{(x_1 - x_2)^2 + (y_1 - y_2)^2} \\ h &= \sqrt{(x_3 - x_3)^2 + (y_1 - y_2)^2} \end{aligned} \quad (7)$$

As shown in the above equation, we term the anchor point  $(x_a, y_a)$  as positive anchor if it satisfies  $|x_a - x_c| < \alpha \times w$  and  $|y_a - y_c| < \alpha \times h$ ; otherwise the point will be termed as ignored point. The above mentioned  $\alpha$  is an experiential hyper-parameter, we set it as 0.8 usually. The above process is presented in Fig. 8.

We show the overall framework RSDet++ in Fig. 7, which can be summarized into three parts. Firstly, we employ a Res50-based feature pyramid network as a baseline which has been widely employed in previous object detection methods such as RetinaNet [15], R2CNN [23], and FCOS [20] for its ability to focus on multi-scale objects. Secondly, an eight-param modulated rotation loss is employed to associate with RSDet++, which can alleviate the rotation sensitivity error. Finally, a point-based sample selection strategy is employed to avoid the tiny trouble in anchor-based methods.

## IV. EXPERIMENTS

To validate the effectiveness of the proposed approaches, we conduct extensive experiments and compare with the recent state-of-the-art methods on several challenging public benchmarks such as aerial images (DOTA, HRSC2016, and

UCAS-AOD), scene text images (ICDAR2015). Tensorflow is employed to implement our proposed methods on a server with V100 and 16 G memory. The experiments in this article are initialized by ResNet50 by default unless otherwise specified. Recall that the main contribution of this paper is to identify the problem of RSE, the introduction of modulated rotation loss, and point-based RSDet++ for tiny objects.

### A. Datasets and Implementation Details

**DOTA [1]:** We carry out the main experiments on the DOTA benchmark that has a total of 2,806 aerial images and 15 categories. The size of images in DOTA ranges from  $800 \times 800$  pixels to  $4,000 \times 4,000$  pixels. The proportions of the training set, the validation set, and the test set are respectively 1/2, 1/6, and 1/3. There are 188,282 instances for training and validation, and they are labeled clockwise with a quadrilateral. Due to the large size of a single aerial image, we divide the image into  $600 \times 600$  pixel sub-images with a 150-pixel overlap between two neighboring ones, and we scale these sub-images to  $800 \times 800$  eventually. There exists three different version of DOTA benchmark: DOTA-v1.0, DOTA-v1.5, and DOTA-v2.0. DOTA-v1.5 and DOTA-v2.0 use the same images as DOTA-v1.0, but the tiny instances (smaller than 10 pixels) are included.

**ICDAR2015 [4]:** ICDAR15 is a scene text dataset that includes 1,500 images, 1000 for training and the remaining for testing. The size of the images in this dataset is  $720 \times 1280$ , and the source of the images is street view. The annotation of the text in an image is four clockwise point coordinates of a quadrangle.

**HRSC2016 [3]:** HRSC2016 is a dataset for ship detection which has a large aspect ratio and arbitrary orientation. This dataset contains two scenarios: ship on sea and ship close inshore. The size of each image ranges from  $300 \times 300$  to  $1,500 \times 900$ . This dataset has 1,061 images including 436 images for training, 181 for validation, and 444 for testing.

**UCAS-AOD [2]:** UCAS-AOD is a remote sensing dataset that contains two categories: car and plane. UCAS-AOD contains 1510 aerial images, each of which has approximately  $659 \times 1,280$  pixels. In line with [30] and [29], we select 1110 images for training and 400 for testing randomly.

**Baselines and Training Details.** To make the experimental results more reliable, the baseline we chose is a multi-class rotated object detector based on RetinaNet, which has been verified in work [32]. During training, we use RetinaNet-Res50, RetinaNet-Res101, and RetinaNet-Res152 [15] for experiments. Our network is initialized with the pre-trained ResNet50 [37] for object classification in ImageNet [38] which is officially published by TensorFlow. Besides, weight decay and momentum are correspondingly  $1e-4$  and 0.9. The training epoch is 30 in total, and the number of iterations per epoch depends on the number of samples in the dataset. The initial learning rate is  $5e-4$ , and the learning rate changes from  $5e-5$  at epoch 18 to  $5e-6$  at epoch 24. We adopt the warm-up strategy to find a suitable learning rate in the first quarter of the training epochs. In inference, rotating non-maximum suppression (R-NMS) is used for post-processing the final detection results.

TABLE I  
ABLATION EXPERIMENTS OF  $\ell_{mr}$  AND PREDEFINED EIGHT-PARAMETER REGRESSION ON DOTA BENCHMARK.

Backbone	Loss	Regression	mAP
resnet-50	smooth- $\ell_1$	five-param.	62.14
resnet-50	$\ell_{mr}$	five-param.	64.49
resnet-50	smooth- $\ell_1$	eight-param.	65.59
resnet-50	$\ell_{mr}$	eight-param.	<b>66.77</b>

TABLE II  
ABLATION EXPERIMENTS OF  $\ell_{mr}$  IN RSDet++ ON DOTA BENCHMARK.

	Backbone	Loss	Regression	mAP
RSDet wo.mr	resnet-50	smooth- $\ell_1$	eight-param.	66.05
RSDet w.mr	resnet-50	$\ell_{mr}$	eight-param.	67.20
RSDet++ wo.mr	resnet-50	smooth- $\ell_1$	eight-param.	67.91
RSDet++ w.mr	resnet-50	$\ell_{mr}$	eight-param.	68.24

### B. Ablation Study

**Ablation Study of Modulated Rotation Loss in 5-parameter and 8-parameter settings.** We use the ResNet50-based RetinaNet-H as our baseline to verify the effectiveness of modulated rotation loss  $\ell_{mr}$ . We get a gain of 2.35% mAP, when the loss function is changed from the smooth- $\ell_1$  loss to  $\ell_{mr}$ , as shown in Table. I. Fig. 2 compares results before and after solving the RSE problem: some objects in the images are all in the boundary case where the loss function is not continuous. A lot of inaccurate results (see red squares in Fig. 2(a) and Fig. 2(c)) are predicted in the baseline method, but these do not occur after using  $\ell_{mr}$  (see the same location in Fig. 2(b) and Fig. 2(d)). Similarly, an improvement of 1.18% mAP is obtained after using the eight-parameter  $\ell_{mr}$ . This set of ablation experiments prove that  $\ell_{mr}$  is effective for improving the rotated object detector. Note the number of parameters and calculations added by these two techniques are almost negligible.

**Ablation Study of Modulated Rotation loss on RSDet++.** The experiments in Table. I show that our modulated rotation loss can enhance the performance of existing rotated object detection methods suffered from the discontinuity of loss. For solving the tiny trouble in anchor-based object detection methods, we introduce the point-based RSDet++ to regress the rotated bounding box from pixels on the feature map. However, the discontinuity of loss also exists in RSDet++. We compare the performance of RSDet++ with modulated rotation loss (RSDet++ w.mr) and RSDet++ without modulated rotation loss (RSDet++ wo.mr) in Table. II, the results shows that modulated rotation loss also works on RSDet++ which improve the baseline from 67.91% to 68.24%.

**Ablation Study of Backbone, Data Augmentation, and Data Balance.** Data augmentation can improve model performance effectively, and we use augmentations including random horizontal flipping, random vertical flipping, random image graying, and random rotation. Consequently, the baseline performance increased by 4.22% to 70.79% on DOTA. Moreover, data imbalance is severe in the DOTA. For instance, there are 76,833 ship instances in the dataset, but there are only 962 ground track fields. We extend samples less than 10,000

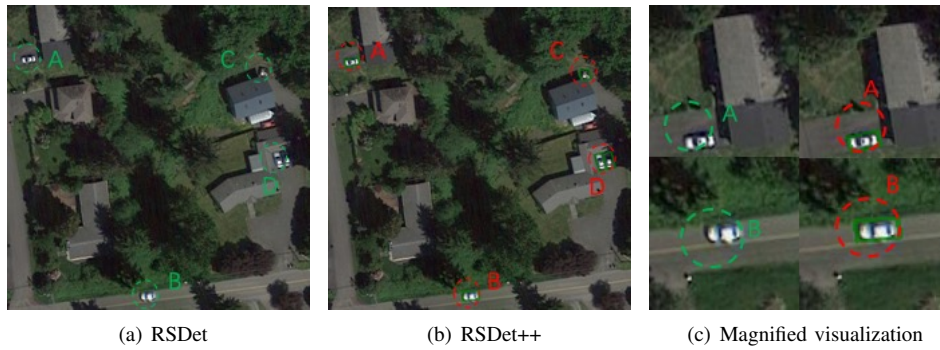


Fig. 9. Visualization of the tiny object detection ability between our RSDet and RSDet++, where the circles localize the ground-truth objects, and A/B/C/D represents different objects. For a clear comparison, we enlarge the local regions A and B in subfigure c, and conclude that the same object neglected in RSDet can be detected in RSDet++.

TABLE III  
ABLATION EXPERIMENTS OF BACKBONE, DATA AUGMENTATION AND BALANCE ON DOTA. RSDet IS THE BASE MODEL.

Backbone	Data Aug	Balance	mAP
resnet-50			66.77
resnet-50	✓		70.79
resnet-50	✓	✓	71.22
resnet-101	✓	✓	72.16
resnet-152	✓	✓	<b>73.51</b>

to 10,000 in each category by random copying, which brings a 0.43% boost, and the most prominent contribution is from a small number of samples, e.g., helicopter and swimming pool. We also explore the impact of different backbones and conclude that a greater backbone brings more performance gains. Performances of the detectors based on ResNet50, ResNet101, and ResNet152 are respectively 71.22%, 72.16% and 73.51%. Refer to Table. III for details.

**Ablation Study of Two-stage Detectors as Base Model.** To prove that  $\ell_{mr}$  can cooperate with other existing frameworks, we apply  $\ell_{mr}$  to the two-stage methods such as RSDet-II and Faster RCNN. By comparison, the  $\ell_{mr}$  achieves consistent improvement on RSDet-II and Faster RCNN. We conduct Faster RCNN based on five-parameter and eight-parameter systems, while RSDet-II only conducts on a five-parameter system. Taking Faster RCNN as an example, it outperforms baseline by 1.6% and 2.84% in mAP after cooperating with  $\ell_{mr}$  in five-parameter and eight-parameter, respectively. The results of RSDet-II are presented in Table. VIII, which reach state-of-the-art on the DOTA benchmark.

**Ablation Study of RSDet and RSDet++.** We compare RSDet and RSDet++ as shown in Table. II, and select the same backbone ResNet50 and eight-parameter regression system for a fair comparison. We note that the performance of RSDet++ both with/without modulated rotation loss are both significantly better than that of RSDet. When comparing the methods without modulated rotation loss, RSDet++ receives 67.91% mAP that is 1.86% higher than RSDet; when comparing the methods with modulated rotation loss, RSDet++ receives 68.24% mAP that is 1.04% higher than RSDet. The above experiments show that when we improve the performance of our methods on tiny objects, point-based methods can achieve better performance than anchor-based methods with a more efficient inference process. We explain the gap that the

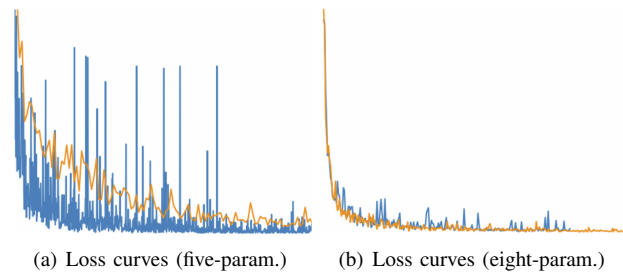


Fig. 10. Comparisons of loss curves during training: where blue for L1-loss and yellow for our loss.

RSDet++ uses a point-based sample selection mode which is more suitable for tiny objects than the traditional IOU-based sample selection mode in anchor-based methods. Moreover, anchor-free methods can provide a more efficient inference process.

In Fig. 9, we also visualize the detection results using the anchor-based RSDet and point-free RSDet++ respectively. We can find that RSDet++ can predict the bounding box of small objects while RSDet can't.

### C. Further Analysis

**Training Stability.** We have analyzed that the discontinuity of loss affects the training stability and the detection performance. Although the detection performances of our methods are verified through mAP, we have not proven the stability improvement of model training brought by our techniques. To this end, we plot the training loss curves using models including RetinaNet-H ( $\ell^{5p}$ ), RSDet-I ( $\ell^{5p}_{mr}$ ), RetinaNet-H ( $\ell^{8p}$ ), and RSDet-I ( $\ell^{8p}_{mr}$ ), as shown in Fig. 10. The training process converges more stable when associating with a modulated rotation loss.

**Comparison with Similar Methods.** Although we introduce the concept of RSE for the first time, it is worth noting that some previous articles have also mentioned similar problems. In [1], they use a 180-degree definition to eliminate the loss burst caused by the exchangeability of height and width. While related works [24], [39] use periodic trigonometric functions to eliminate the effects of the angular periodicity. SCRDet [31] proposes IoU-smooth- $\ell_1$  loss to solve the boundary discontinuity. However, these methods are limited and do not completely solve the RSE problem. Our method yields the

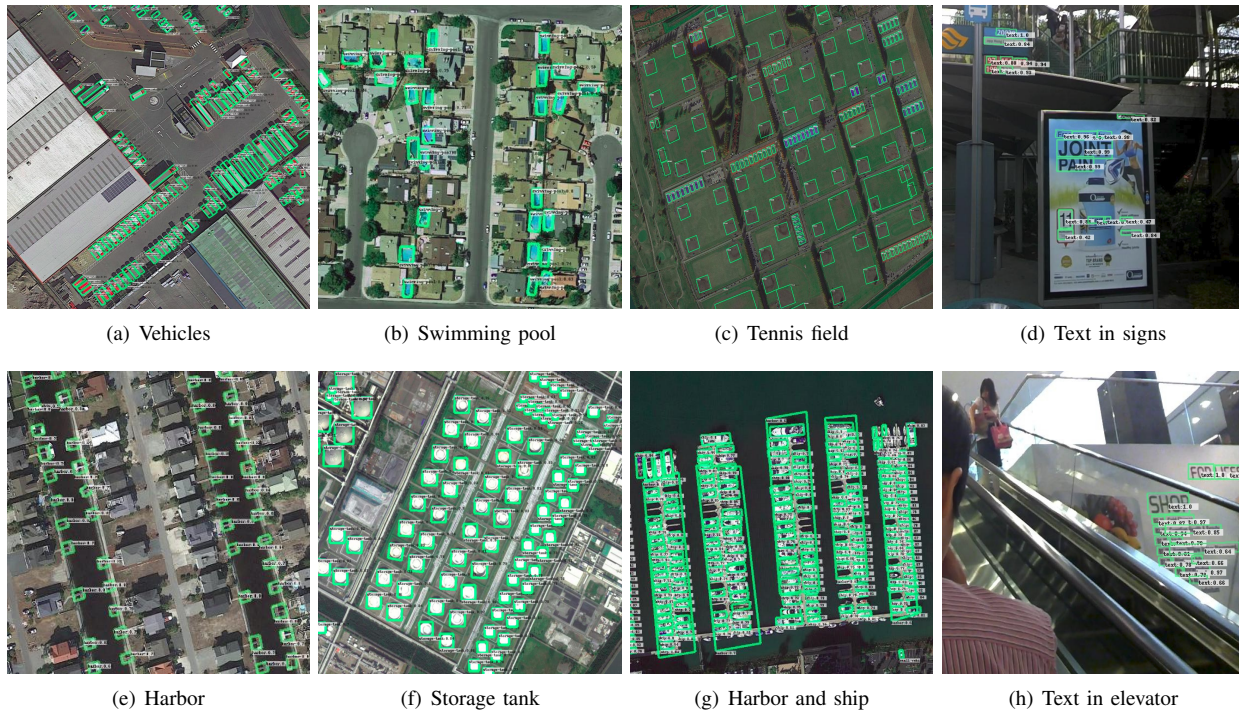


Fig. 11. Detection results on DOTA and ICDAR15.

TABLE IV  
ABLATION STUDY USING THE PROPOSED TECHNIQUES ON DOTA.  
RETINANET-H[32] IS THE BASE MODEL.

Loss	Regression	mAP
smooth- $\ell_1$	five-param. $[-\frac{\pi}{2}, 0)$	62.14
smooth- $\ell_1$ [1]	five-param. $[-\pi, 0)$	62.39
IoU-smooth- $\ell_1$ [31]	five-param. $[-\frac{\pi}{2}, 0)$	62.69
$\ell_{mr}$	five-param. $[-\frac{\pi}{2}, 0)$	64.49
smooth- $\ell_1$	eight-param.	65.59
$\ell_{mr}$	eight-param.	<b>66.77</b>

TABLE V  
PERFORMANCES OF  $\ell_{mr}$  AND EIGHT-PARA. REGRESSION ON ICDAR2015  
AND HRSC2016. USE RETINANET-H [32] AS BASE MODEL, AND  
RESNET152 BACKBONE.

Loss	Regression	ICDAR2015	HRSC2016
smooth- $\ell_1$	five-param.	76.8	82.4
$\ell_{mr}$	five-param.	79.6	83.6
smooth- $\ell_1$	eight-param.	81.2	85.4
$\ell_{mr}$	eight-param.	<b>83.2</b>	<b>86.5</b>

TABLE VI  
PERFORMANCE ON DOTA1.5 AND DOTA2.0.

Method	Box Def.	DOTA-V1.5	DOTA-v2.0
IOU-smooth L1 [31]	$D_{oc}$	59.16	46.31
RIDet [40]	quad.	58.91	45.35
CSL [35]	$D_{oc}$	58.55	43.34
DCL [41]	$D_{oc}$	59.38	45.46
GWD [42]	$D_{oc}$	60.03	46.65
KLD [43]	$D_{oc}$	62.50	47.69
RSDet	quad.	61.42	46.71
RSDet++	quad.	62.18	48.81

most promising results when comparing with these methods as shown in Table. IV.

**Performances on Other Datasets.** We further do experi-

TABLE VII  
ACCURACY COMPARISON BETWEEN DIFFERENT ROTATION DETECTORS ON  
DOTA DATASET. THE BOLD RED FONTS INDICATE THE TOP ONE  
PERFORMANCES RESPECTIVELY.  $D_{oc}$  AND  $D_{le}$  REPRESENT OPENCV  
DEFINITION ( $\theta \in [-90^\circ, 0^\circ)$ ) AND LONG EDGE DEFINITION  
( $\theta \in [-90^\circ, 90^\circ)$ ) OF RBOX.

Method	Box Def.	v1.0 train/val		
		AP <sub>50</sub>	AP <sub>75</sub>	AP <sub>50:95</sub>
Retina Baseline	$D_{oc}$	64.70	32.31	34.50
Retina Baseline	$D_{le}$	62.21	26.06	31.49
IoU-Smooth L1 [31]	$D_{oc}$	64.61	34.17	36.23
CSL [35]	$D_{le}$	64.40	32.58	35.04
DCL (BCL) [41]	$D_{le}$	65.93	35.66	36.71
Modulated Loss (ours)	$D_{oc}$	63.50	33.32	34.61
Modulated Loss (ours)	Quad.	65.15	<b>40.59</b>	<b>39.12</b>

ments on ICDAR2015, and HRSC2016 as shown in Table. V. For ICDAR2015, there are rich existing methods such as R<sup>2</sup>CNN, Deep direct regression [51] and FOTS [52], and the current state-of-art has reached 91.67%. Although they use many text-based tricks, we notice that they are also not aware of the rotation sensitivity error. Therefore, we conduct some verification experiments based on  $\ell_{mr}$ , and we achieve improvements on both datasets. Our detector achieves competitive results and shows its generalization on scene text data. Besides, we also experiment with the modulated loss on HRSC2016, and the experimental results are comparable to state-of-art.

**Performance of RSDet++ on DOTA1.5 and DOTA2.0.**

Table VI reports the performance of RSDet++ and other previous state-of-the-art rotation object detection methods on DOTA-v1.5 and DOTA-v2.0 such as IOU-smooth L1, RIDet, CSL, DCL, GWD, and KLD. Without bells and whistles, RSDet++ can achieve competitive performance when comparing with other anchor-based methods. For example, RSDet++

TABLE VIII

DETECTION ACCURACY ON DIFFERENT OBJECTS AND OVERALL PERFORMANCES WITH THE STATE-OF-THE-ART METHODS ON DOTA. THE SHORT NAMES FOR CATEGORIES ARE DEFINED AS (ABBREVIATION-FULL NAME): PL-PLANE, BD-BASEBALL DIAMOND, BR-BRIDGE, GTF-GROUND FIELD TRACK, SV-SMALL VEHICLE, LV-LARGE VEHICLE, SH-SHIP, TC-TENNIS COURT, BC-BASKETBALL COURT, ST-STORAGE TANK, SBF-SOCCER-BALL FIELD, RA-ROUNDBOUT, HA-HARBOR, SP-SWIMMING POOL, AND HC-HELICOPTER. BB MEANS BACKBONE.

Method	BB	Reg.	PL	BD	BR	GTF	SV	LV	SH	TC	BC	ST	SBF	RA	HA	SP	HC	mAP
<b>Two-stage</b>																		
IENet [44]	R-101	6p	80.2	64.5	39.8	32.0	49.7	65.0	52.6	81.5	44.7	78.5	46.5	56.7	64.4	64.2	36.8	57.1
R-DFPN [45]	R-101	5p	80.9	65.8	33.8	58.9	55.8	50.9	54.8	90.3	66.3	68.7	48.7	51.8	55.1	51.3	35.9	57.9
R <sup>2</sup> CNN [23]	R-101	5p	80.9	65.7	35.3	67.4	59.9	50.9	55.8	90.7	66.9	72.4	55.1	52.2	55.1	53.4	48.2	60.7
RRPN [24]	R-101	5p	88.5	71.2	31.7	59.3	51.9	56.2	57.3	90.8	72.8	67.4	56.7	52.8	53.1	51.9	53.6	61.0
ICN [29]	R-101	5p	81.4	74.3	47.7	70.3	64.9	67.8	70.0	90.8	79.1	78.2	53.6	62.9	67.0	64.2	50.2	68.2
RoI Trans. [30]	R-101	5p	88.6	78.5	43.4	75.9	68.8	73.7	83.6	90.7	77.3	81.5	58.4	53.5	62.8	58.9	47.7	69.6
CAD-Net [46]	R-101	5p	87.8	82.4	49.4	73.5	71.1	63.5	76.7	90.9	79.2	73.3	48.4	60.9	62.0	67.0	62.2	69.9
SCRDet [31]	R-101	5p	89.9	80.7	52.1	68.4	68.4	60.3	72.4	90.9	87.9	86.9	65.0	66.7	66.3	68.2	65.2	72.6
Gliding Ver. [33]	R-101	9p	89.6	85.0	52.3	<b>77.3</b>	73.0	73.1	86.8	90.7	79.0	86.8	59.6	70.9	72.9	70.9	57.3	75.0
FFA [36]	R-101	5p	90.1	82.7	54.2	75.2	71.0	<b>79.9</b>	83.5	90.7	83.9	84.6	61.2	68.0	70.7	76.0	63.7	75.7
APE [47]	R-101	5p	89.9	83.6	53.4	76.0	74.0	77.2	79.5	90.8	87.2	84.5	67.7	60.3	74.6	71.8	65.6	75.8
CenterMap [34]	R-101	5p	89.8	84.4	54.6	70.3	<b>77.7</b>	78.3	<b>87.2</b>	90.7	84.9	85.3	56.5	69.2	74.1	71.6	66.1	76.0
RSDet-II	R-152	8p	89.9	<b>84.5</b>	53.8	74.4	71.5	78.3	78.1	91.1	87.4	<b>86.9</b>	65.6	65.2	<b>75.4</b>	<b>79.7</b>	63.3	<b>76.3</b>
<b>One-stage</b>																		
P-RSDet [48]	R-101	3p	89.0	73.7	47.3	72.0	70.6	73.7	72.8	90.8	80.1	81.3	59.5	57.9	60.8	65.2	52.6	69.8
O <sup>2</sup> -DNet [49]	H-104	10p	89.3	82.1	47.3	61.2	71.3	74.0	78.6	90.8	82.2	81.4	60.9	60.2	58.2	66.9	61.0	71.0
DRN [50]	H-104	5p	89.7	82.3	47.2	64.1	76.2	74.4	85.8	90.6	86.2	84.9	57.7	61.9	69.3	69.6	58.5	73.2
R <sup>3</sup> Det [32]	R-152	5p	89.5	81.2	50.5	66.1	70.9	78.7	78.2	90.8	85.3	84.2	61.8	63.8	68.2	69.8	67.2	73.7
RSDet-I	R-152	8p	<b>90.0</b>	<b>83.9</b>	<b>54.7</b>	69.9	70.6	79.6	75.4	<b>91.2</b>	<b>88.0</b>	85.6	65.2	<b>69.2</b>	67.0	70.2	64.6	75.0
RSDet++	R-152	8p	86.8	82.7	54.6	71.7	76.0	71.2	83.5	87.4	83.4	85.3	<b>72.4</b>	62.9	70.9	72.3	<b>70.4</b>	<b>75.4</b>

employs an anchor-free backbone which is more efficient and outperforms the second-best method KLD by 1.12% mAP on DOTA-v2.0 while also achieves competitive results with KLD on DOTA-v1.5.

**High Precision Protocol of Modulated Loss.** As aforementioned, our proposed RSDet++ show better performance on tiny objects than pervious anchor-based methods. Moreover, we evaluate RSDet++ on some high precision protocols such as  $AP_{75}$  and  $AP_{50:95}$  in Table VII, and find that quadrilateral-based Modulated Loss achieves higher performance than other methods such as IoU-Smooth L1 [31], CSL [35], and DCL [41]. For example, the quadrilateral-based Modulated Loss achieves 40.59% on  $AP_{75}$  which outperforms the DCL by a large marge 4.93%, a similar result can be achieved on  $AP_{50:95}$  which outperforms the DCL by a large marge 2.41%.

#### D. Overall Evaluation

The results on DOTA1.0 are shown in Table VIII. The compared methods include i) one-stage methods: P-RSDet [48], O<sup>2</sup>-DNet [49], DRN [50], R<sup>3</sup>Det [32] ii) two-stage methods: R<sup>2</sup>CNN [23], Gliding Vertex [33], FFA [36], APE [47], CenterMap OBB [34]. The results of DOTA are all obtained by submitting predictions to the official evaluation server. We apply  $\ell_{mr}$  to the one-stage and two-stage approaches, and call them RSDet-I and RSDet-II, respectively. In the one-stage methods, RSDet-I obtained 75.03% mAP, which is 1.29% higher than the existing best method (R<sup>3</sup>Det). And in the two-stage methods, RSDet-II obtained 76.34% mAP, which is 0.31% higher than CenterMap OBB, 1.28% higher than Gliding Vertex. Table. IX gives the comparison on the UCAS-AOD dataset, where our method achieves 96.50% for the OBB task that outperforms all the published methods. Moreover, the number of parameters and calculations added by our techniques are almost negligible, and they can be applied

TABLE IX  
PERFORMANCE EVALUATION ON UCAS-AOD DATASET.

Method	Plane	Car	mAP
YOLOv2 [12]	96.60	79.20	87.90
R-DFPN [45]	95.90	82.50	89.20
DRBox [53]	94.90	85.00	89.95
S <sup>2</sup> ARN [39]	97.60	92.20	94.90
RetinaNet-H [32]	97.34	93.60	95.47
ICN [29]	-	-	95.67
FADet [54]	98.69	92.72	95.71
R <sup>3</sup> Det [32]	98.20	94.14	96.17
Ours	<b>98.04</b>	<b>94.97</b>	<b>96.50</b>

to all region-based rotation detection algorithms. Visualization results are shown in Fig. 11.

#### V. CONCLUSION

In this paper, the issue of rotation sensitivity error (RSE) is formally identified and formulated for region-based rotated object detectors. RSE mainly refers to the discontinuity of loss which caused by the contradiction between the definition of the rotated bounding box and the loss function. A novel modulated rotation loss  $\ell_{mr}$  is proposed to address the discontinuity of loss in five-parameter and eight-parameter methods. To prove the effectiveness of modulated loss, we conduct experiments based on one-stage and two-stage methods respectively. Moreover, we further propose a RSDet++ to improve the performance on tiny objects based on a point-based bounding box regression approach. Extensive experiments demonstrate that RSDet achieves state-of-art performance on the DOTA1.0 benchmark and RSDet++ performs better on DOTA1.5 and DOTA2.0 which focus more on tiny objects.

## VI. ACKNOWLEDGMENT

This research is supported by The Commercialization of Research Findings Fund of Inner Mongolia Autonomous Region (2020CG0075). The author Wen Qian is supported by Multidimensional Data Analysis Laboratory, Institute of Automation, Chinese Academy of Sciences.

## REFERENCES

- [1] G.-S. Xia, X. Bai, J. Ding, Z. Zhu, S. Belongie, J. Luo, M. Datcu, M. Pelillo, and L. Zhang, "Dota: A large-scale dataset for object detection in aerial images," in *Proceedings of the IEEE conference on computer vision and pattern recognition*, 2018, pp. 3974–3983.
- [2] H. Zhu, X. Chen, W. Dai, K. Fu, Q. Ye, and J. Jiao, "Orientation robust object detection in aerial images using deep convolutional neural network," in *IEEE International Conference on Image Processing*. IEEE, 2015, pp. 3735–3739.
- [3] Z. Liu, L. Yuan, L. Weng, and Y. Yang, "A high resolution optical satellite image dataset for ship recognition and some new baselines," pp. 324–331, 2017.
- [4] D. Karatzas, L. Gomez-Bigorda, A. Nicolaou, S. Ghosh, A. Bagdanov, M. Iwamura, J. Matas, L. Neumann, V. R. Chandrasekhar, S. Lu *et al.*, "Icdar 2015 competition on robust reading," in *2015 13th International Conference on Document Analysis and Recognition*. IEEE, 2015, pp. 1156–1160.
- [5] R. Gomez, B. Shi, L. Gomez, L. Numann, A. Veit, J. Matas, S. Belongie, and D. Karatzas, "Icdar2017 robust reading challenge on coco-text," in *2017 14th IAPR International Conference on Document Analysis and Recognition*, vol. 1. IEEE, 2017, pp. 1435–1443.
- [6] W. Qian, X. Yang, S. Peng, J. Yan, and Y. Guo, "Learning modulated loss for rotated object detection," in *Thirty-Fifth AAAI Conference on Artificial Intelligence, AAAI 2021, Thirty-Third Conference on Innovative Applications of Artificial Intelligence, IAAI 2021, The Eleventh Symposium on Educational Advances in Artificial Intelligence, EAAI 2021, Virtual Event, February 2-9, 2021*. AAAI Press, 2021, pp. 2458–2466. [Online]. Available: <https://ojs.aaai.org/index.php/AAAI/article/view/16347>
- [7] R. Girshick, J. Donahue, T. Darrell, and J. Malik, "Rich feature hierarchies for accurate object detection and semantic segmentation," in *Proceedings of the IEEE conference on computer vision and pattern recognition*, 2014, pp. 580–587.
- [8] R. Girshick, "Fast r-cnn," in *The IEEE International Conference on Computer Vision*, 2015, pp. 1440–1448.
- [9] S. Ren, K. He, R. B. Girshick, and J. Sun, "Faster R-CNN: towards real-time object detection with region proposal networks," *IEEE Trans. Pattern Anal. Mach. Intell.*, vol. 39, no. 6, pp. 1137–1149, 2017.
- [10] J. Dai, Y. Li, K. He, and J. Sun, "R-fcn: Object detection via region-based fully convolutional networks," in *Advances in neural information processing systems*, 2016, pp. 379–387.
- [11] P. Sermanet, D. Eigen, X. Zhang, M. Mathieu, R. Fergus, and Y. LeCun, "Overfeat: Integrated recognition, localization and detection using convolutional networks," in *2nd International Conference on Learning Representations*, Y. Bengio and Y. LeCun, Eds., 2014.
- [12] J. Redmon, S. Divvala, R. Girshick, and A. Farhadi, "You only look once: Unified, real-time object detection," in *Proceedings of the IEEE conference on computer vision and pattern recognition*, 2016, pp. 779–788.
- [13] W. Liu, D. Anguelov, D. Erhan, C. Szegedy, S. Reed, C.-Y. Fu, and A. C. Berg, "Ssd: Single shot multibox detector," in *Proceedings of the European Conference on Computer Vision*. Springer, 2016, pp. 21–37.
- [14] T.-Y. Lin, P. Dollár, R. Girshick, K. He, B. Hariharan, and S. Belongie, "Feature pyramid networks for object detection," in *Proceedings of the IEEE conference on computer vision and pattern recognition*, 2017, pp. 2117–2125.
- [15] T. Y. Lin, P. Goyal, R. Girshick, K. He, and P. Dollár, "Focal loss for dense object detection," *IEEE transactions on pattern analysis and machine intelligence*, vol. PP, no. 99, pp. 2999–3007, 2017.
- [16] C. Fu, W. Liu, A. Ranga, A. Tyagi, and A. C. Berg, "DSSD : Deconvolutional single shot detector," *CoRR*, vol. abs/1701.06659, 2017.
- [17] Z. Cai and N. Vasconcelos, "Cascade r-cnn: Delving into high quality object detection," in *Proceedings of the IEEE conference on computer vision and pattern recognition*, 2018, pp. 6154–6162.
- [18] K. Chen, J. Pang, J. Wang, Y. Xiong, X. Li, S. Sun, W. Feng, Z. Liu, J. Shi, W. Ouyang *et al.*, "Hybrid task cascade for instance segmentation," in *Proceedings of the IEEE conference on computer vision and pattern recognition*, 2019, pp. 4974–4983.
- [19] S. Zhang, L. Wen, X. Bian, Z. Lei, and S. Z. Li, "Single-shot refinement neural network for object detection," in *Proceedings of the IEEE conference on computer vision and pattern recognition*, 2018, pp. 4203–4212.
- [20] Z. Tian, C. Shen, H. Chen, and T. He, "FCOS: fully convolutional one-stage object detection," in *2019 IEEE/CVF International Conference on Computer Vision, ICCV 2019, Seoul, Korea (South), October 27 - November 2, 2019*. IEEE, 2019, pp. 9626–9635.
- [21] T. Kong, F. Sun, H. Liu, Y. Jiang, and J. Shi, "Foveabox: Beyond anchor-based object detector," *CoRR*, vol. abs/1904.03797, 2019. [Online]. Available: <http://arxiv.org/abs/1904.03797>
- [22] Z. Yang, S. Liu, H. Hu, L. Wang, and S. Lin, "Reppoints: Point set representation for object detection," in *2019 IEEE/CVF International Conference on Computer Vision*. IEEE, 2019, pp. 9656–9665.
- [23] Y. Jiang, X. Zhu, X. Wang, S. Yang, W. Li, H. Wang, P. Fu, and Z. Luo, "R2CNN: rotational region CNN for orientation robust scene text detection," *CoRR*, vol. abs/1706.09579, 2017. [Online]. Available: <http://arxiv.org/abs/1706.09579>
- [24] J. Ma, W. Shao, H. Ye, L. Wang, H. Wang, Y. Zheng, and X. Xue, "Arbitrary-oriented scene text detection via rotation proposals," *IEEE Transactions on Multimedia*, vol. 20, no. 11, pp. 3111–3122, 2018.
- [25] K. Fu, Y. Li, H. Sun, X. Yang, G. Xu, Y. Li, and X. Sun, "A ship rotation detection model in remote sensing images based on feature fusion pyramid network and deep reinforcement learning," *Remote Sensing*, vol. 10, no. 12, p. 1922, 2018.
- [26] X. Yang, K. Fu, H. Sun, X. Sun, M. Yan, W. Diao, and Z. Guo, "Object detection with head direction in remote sensing images based on rotational region cnn," in *IGARSS 2018-2018 IEEE International Geoscience and Remote Sensing Symposium*. IEEE, 2018, pp. 2507–2510.
- [27] J. Yang, L. Ji, X. Geng, X. Yang, and Y. Zhao, "Building detection in high spatial resolution remote sensing imagery with the u-rotation detection network," *International Journal of Remote Sensing*, vol. 40, no. 15, pp. 6036–6058, 2019.
- [28] M. Liao, B. Shi, and X. Bai, "Textboxes++: A single-shot oriented scene text detector," *IEEE transactions on image processing*, vol. 27, no. 8, pp. 3676–3690, 2018.
- [29] S. M. Azimi, E. Vig, R. Bahmanyar, M. Körner, and P. Reinartz, "Towards multi-class object detection in unconstrained remote sensing imagery," in *Asian Conference on Computer Vision*. Springer, 2018, pp. 150–165.
- [30] J. Ding, N. Xue, Y. Long, G. Xia, and Q. Lu, "Learning roi transformer for oriented object detection in aerial images," in *IEEE Conference on Computer Vision and Pattern Recognition*. Computer Vision Foundation / IEEE, 2019, pp. 2849–2858.
- [31] X. Yang, J. Yang, J. Yan, Y. Zhang, T. Zhang, Z. Guo, X. Sun, and K. Fu, "Scrnet: Towards more robust detection for small, cluttered and rotated objects," in *2019 IEEE/CVF International Conference on Computer Vision*. IEEE, 2019, pp. 8231–8240.
- [32] X. Yang, Q. Liu, J. Yan, and A. Li, "R3det: Refined single-stage detector with feature refinement for rotating object," *arXiv preprint arXiv:1908.05612*, 2019.
- [33] Y. Xu, M. Fu, Q. Wang, Y. Wang, and X. Bai, "Gliding vertex on the horizontal bounding box for multi-oriented object detection," *IEEE Transactions on Pattern Analysis and Machine Intelligence*, vol. PP, no. 99, pp. 1–1, 2020.
- [34] J. Wang, W. Yang, H.-C. Li, H. Zhang, and G.-S. Xia, "Learning center probability map for detecting objects in aerial images," *IEEE Transactions on Geoscience and Remote Sensing*, 2020.
- [35] X. Yang, J. Yan, and T. He, "On the arbitrary-oriented object detection: Classification based approaches revisited," *arXiv preprint arXiv:2003.05597*, 2020.
- [36] K. Fu, Z. Chang, Y. Zhang, G. Xu, K. Zhang, and X. Sun, "Rotation-aware and multi-scale convolutional neural network for object detection in remote sensing images," *ISPRS Journal of Photogrammetry and Remote Sensing*, vol. 161, pp. 294–308, 2020.
- [37] K. He, X. Zhang, S. Ren, and J. Sun, "Deep residual learning for image recognition," in *Proceedings of the IEEE conference on computer vision and pattern recognition*, 2016, pp. 770–778.
- [38] J. Deng, W. Dong, R. Socher, L.-J. Li, K. Li, and L. Fei-Fei, "Imagenet: A large-scale hierarchical image database," in *Proceedings of the IEEE conference on computer vision and pattern recognition*. IEEE, 2009, pp. 248–255.

- [39] S. Bao, X. Zhong, R. Zhu, X. Zhang, Z. Li, and M. Li, "Single shot anchor refinement network for oriented object detection in optical remote sensing imagery," *IEEE Access*, vol. 7, pp. 87 150–87 161, 2019.
- [40] Q. Ming, Z. Zhou, L. Miao, X. Yang, and Y. Dong, "Optimization for oriented object detection via representation invariance loss," *arXiv preprint arXiv:2103.11636*, 2021.
- [41] X. Yang, L. Hou, Y. Zhou, W. Wang, and J. Yan, "Dense label encoding for boundary discontinuity free rotation detection," *CoRR*, vol. abs/2011.09670, 2020. [Online]. Available: <https://arxiv.org/abs/2011.09670>
- [42] X. Yang, J. Yan, Q. Ming, W. Wang, X. Zhang, and Q. Tian, "Rethinking rotated object detection with gaussian wasserstein distance loss," *arXiv preprint arXiv:2101.11952*, 2021.
- [43] X. Yang, X. Yang, J. Yang, Q. Ming, W. Wang, Q. Tian, and J. Yan, "Learning high-precision bounding box for rotated object detection via kullback-leibler divergence," *arXiv preprint arXiv:2106.01883*, 2021.
- [44] Y. Lin, P. Feng, and J. Guan, "Ienet: Interacting embranchment one stage anchor free detector for orientation aerial object detection," *arXiv preprint arXiv:1912.00969*, 2019.
- [45] X. Yang, H. Sun, K. Fu, J. Yang, X. Sun, M. Yan, and Z. Guo, "Automatic ship detection in remote sensing images from google earth of complex scenes based on multiscale rotation dense feature pyramid networks," *Remote Sensing*, vol. 10, no. 1, p. 132, 2018.
- [46] G. Zhang, S. Lu, and W. Zhang, "Cad-net: A context-aware detection network for objects in remote sensing imagery," *IEEE Transactions on Geoscience and Remote Sensing*, vol. 57, no. 12, pp. 10 015–10 024, 2019.
- [47] Y. Zhu, J. Du, and X. Wu, "Adaptive period embedding for representing oriented objects in aerial images," *IEEE Transactions on Geoscience and Remote Sensing*, vol. 58, no. 10, pp. 7247–7257, 2020.
- [48] L. Zhou, H. Wei, H. Li, Y. Zhang, X. Sun, and W. Zhao, "Objects detection for remote sensing images based on polar coordinates," *arXiv preprint arXiv:2001.02988*, 2020.
- [49] H. Wei, Y. Zhang, Z. Chang, H. Li, H. Wang, and X. Sun, "Oriented objects as pairs of middle lines," *ISPRS Journal of Photogrammetry and Remote Sensing*, vol. 169, pp. 268–279, 2020.
- [50] X. Pan, Y. Ren, K. Sheng, W. Dong, H. Yuan, X. Guo, C. Ma, and C. Xu, "Dynamic refinement network for oriented and densely packed object detection," in *2020 IEEE/CVF Conference on Computer Vision and Pattern Recognition*. IEEE, 2020, pp. 11 204–11 213.
- [51] W. He, X.-Y. Zhang, F. Yin, and C.-L. Liu, "Deep direct regression for multi-oriented scene text detection," in *Proceedings of the IEEE conference on computer vision and pattern recognition*, 2017, pp. 745–753.
- [52] X. Liu, D. Liang, S. Yan, D. Chen, Y. Qiao, and J. Yan, "Fots: Fast oriented text spotting with a unified network," in *Proceedings of the IEEE conference on computer vision and pattern recognition*, 2018, pp. 5676–5685.
- [53] L. Liu, Z. Pan, and B. Lei, "Learning a rotation invariant detector with rotatable bounding box," *CoRR*, vol. abs/1711.09405, 2017. [Online]. Available: <http://arxiv.org/abs/1711.09405>
- [54] C. Li, C. Xu, Z. Cui, D. Wang, T. Zhang, and J. Yang, "Feature-attentioned object detection in remote sensing imagery," in *IEEE International Conference on Image Processing*. IEEE, 2019, pp. 3886–3890.